Scripta Materialia 266 (2025) 116795

Contents lists available at ScienceDirect

Scripta Materialia

journal homepage: www.journals.elsevier.com/scripta-materialia

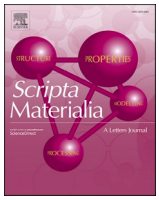

Breakthroughs in scanning electron microscopy poling of massive dense and porous lead-free piezoelectric ceramics

Pietro Galizia [a,*], Alessia Tavolaro [a], Carlo Baldisserri [a], Floriana Craciun [b], Elisa Mercadelli [a]

[a] CNR-ISSMC, National Research Council of Italy - Institute of Science, Technology and Sustainability for Ceramics, Via Granarolo 64, 48018 Faenza, Italy
[b] CNR-ISM, National Research Council of Italy - Institute of Structure of Matter, Via del Fosso del Cavaliere 100, 00133 Tor Vergata, Italy

ARTICLE INFO

Keywords:
Electron beam method
Scanning electron microscopy (SEM)
Ferroelectric ceramics
Piezoelectric ceramics
Poling

ABSTRACT

This study exploits a poling method based on the use of the electron beam in scanning electron microscopy (SEM) to fully activate massive porous and dense piezoelectric ceramics, which are difficult to polarize in high electric fields. Key parameters such as scan speed, exposure time, specimen thickness, and the presence of sputtered electrodes, were analyzed for their effect on the poling process, with d_{33} coefficient measurements used for evaluation. SEM-induced poling activated both dense (410 pC/N) and porous (500 pC/N) lead-free BCTZ ceramics, outperforming traditional oil-based poling (d_{33} < 350 pC/N). This SEM-induced method offers exceptional flexibility and precision, enabling customizable poling patterns without the need for surface electrodes.

The ability of piezoelectric materials to convert mechanical energy into an electrical signal, and vice versa, makes them indispensable in a wide range of devices, such as ultrasound transducers, sensors, actuators capacitors and energy harvesters [1–6]. Currently, there is a growing demand for advanced structures, lightweight, and miniaturized designs with customized architectures [7–12] in some cutting-edge fields, such as multi-dimensional deformation detection, structural health monitoring, smart skin development, purification systems, electrocatalysis, fluid characterizations, spintronic and micro/nano electromechanical systems [13–25]. This requires combining piezoelectric ceramics, with high dielectric constants, alongside phases with low dielectric constant [26–31], which complicates the poling process, especially for materials with intricate geometries [32–35]. As a result, conventional poling often fails to activate piezoelectricity [36,37]. To address this challenge, research has focused on developing new poling techniques, such as corona poling [36,38,39] and alternating current electric field poling (AC-poling) method [40–44]. Moreover, to enhance the electric dipolar order of ferroelectric polymer thin films, which is naturally lower than in crystalline ferroelectrics, scanning force microscopy was used for nanoscale domain writing, i.e. reorientation and alignment of the electric polarization [45,46]. Since 1988, a technique using electron beams within scanning electron microscopes (SEM) has been proposed for polarizing inorganic crystals, as well as polymeric and inorganic thin films. Thus in Refs. [47,48] thin films of polyvinylidene fluoride (PVDF) have been polarized by this technique and the depth profiles of the polarization in the films have been analyzed. It has been found that they depend both on the energy of the incident electrons as well as on the material parameters. Further investigations [49,50] demonstrated the possibility to use this technique for imprinting well-defined polarization patterns, such as a ferroelectric-domain-inverted grating in $LiNbO_3$ crystals of 500 μm thickness, and waveguide devices for second harmonic generation (SHG) for optical applications have been demonstrated. Also in Ref. [51] the electron beam-induced poling of $BaTiO_3$ thin films, using a SEM with different electron beam energies, has been obtained. It has been shown that this technique is effective for nonlinear photonic device fabrication based on writing a periodic pattern directly, by scanning the focused electron beam [52]. A discussion of the electron beam poling mechanisms has been presented in Ref. [52]. It has been found that the velocity of the poling process is determined by the current density and by the material characteristics. For electron beam energy in the range of tens of keV very high electric fields are developed. It has been found, strikingly, that although the electron penetration depth is limited, the polarization can extend over all sample thickness, which can be orders of magnitude higher than the electron penetration depth, which is in the order of some microns. An explanation could be that the beam can induce a region of conducting plasma which advances the potential boundary in the material. Further advancement in the field of electron beam charging and poling by use of SEM has been reported in

* Corresponding author.
E-mail address: pietro.galizia@cnr.it (P. Galizia).

https://doi.org/10.1016/j.scriptamat.2025.116795
Received 9 January 2025; Received in revised form 9 May 2025; Accepted 25 May 2025
Available online 29 May 2025

Ref. [53], where the technique has been applied to thin fluoropolymer layers and the dependence of the generated surface potential on the beam energy has been investigated. Moreover, in this study the successful writing of polarized microdomains in the polymer has been obtained by using computer-controlled electron beam scanning. Electron injection creates an internal electric field between the negatively charged layer—formed by electrons deposited onto the material by the SEM beam—and the back electrode layer. The field strength depends on the electron beam density and the duration of exposure at the incidence location. It is estimated that a spot charge of less than 1 nC forms in the region under the electron beam (see "Localized electrical charge onto a thick dielectric slab" support information). The excellent potential of electron beam poling in SEM to orient or switch the local polarization in ferroelectric materials and thin films has been further employed as a sophisticated technique for imprinting nanoscale domain patterns over large areas, with increased resolution, and the control parameters have been investigated [54–60]. Despite the significant potential of SEM-induced poling, to the best of the authors' knowledge this method has never been applied to massive piezoelectric ceramics, nor has it achieved full polarization. Moreover, the limited d_{33} values reported in the literature are only a fraction of those obtained using traditional poling methods [54,61].

In this study, we investigate the feasibility of performing non-contact (corona poling-like [32]) poling below Curie point and using the electron-beam of a scanning electron microscope (SEM). The key idea is to exploit charge accumulation [62,63], which, due to the poor conductivity of ferroelectric materials, can persist for long periods and generate an electric field capable of polarizing the domains. We applied this technique, for the first time, to pole massive (thickness up to ~ 1 cm) dense and porous piezoelectric ceramics. We focused on lead-free $0.5Ba(Ti_{0.8}Zr_{0.2})O_3-0.5(Ba_{0.7}Ca_{0.3})TiO_3$ solid solution (BTZ–BCT) due to its properties, which are particularly advantageous for the scope of this study. These include a low Curie temperature ($70\ ^\circ C < T_C < 115\ ^\circ C$) [33,64–66], a low coercive field (0.15–0.4 kV/mm) [64,65,67,68], and a low saturation electric field (2–3 kV/mm) [16,65,67,69]. When exposed to an electric field, these materials exhibit changes in rhombohedral–tetragonal phase content and reduced tetragonal distortion, facilitating polarization [67,70]. Moreover, changes in domain morphology of lead-free BTZ–BCT was observed during transmission electron microscopy (TEM) analysis applying an accelerating voltage of 200 kV. After the field was reduced, the domain configurations reappeared [71,72]. It is worth noting that although TEM involves smaller current, in the range of about 50–650 pA, it could damage the material [73]. Lead-free BTZ–BCT piezoelectric ceramics have emerged prominently in the race for improving piezoelectric properties of lead-free materials over the past two decades [68,74–85]. Different studies have been focused on optimizing both composition and process parameters to enhance their performance [86–94]. The BT-based family has garnered significant attention due to its exceptionally high piezoelectric coefficient reaching up to 620 pC/N and theoretically capable of achieving 1500–2000 pC/N [74,95]. Recent studies have explored porous piezoelectric ceramics for fluid microfiltration in applications like water treatment and recovery of bioactive molecules from agro-food waste [15,66,96]. By generating ultrasound, porous piezoelectric membranes could actively improve the antifouling properties of traditional filters. Given the need for lead-free ceramics in these applications, we focused on lead-free BTZ–BCT porous piezoelectric ceramics, aiming to address challenges in polarizing porous samples, which are prone to breakdown under high electric fields. We apply the poling method based on the use of the electron beam in SEM to polarize both porous and dense BTZ–BCT piezoelectric ceramics, comparing the results with conventional electric field poling.

Here, $(Ba_{0.85}Ca_{0.15})(Ti_{0.9}Zr_{0.1})O_3$ powders (BCTZ) were synthetized using the solid state reaction method [97]. $BaCO_3$ (Aldrich purity >99 %), $CaCO_3$ (MERCK purity >99 %), TiO_2 (Degussa P25: purity >99.5 %) and ZrO_2 (MEL, SC 101, purity >99 %) were used as starting materials, ball-milled for 20 h, then pressed and calcinated at 1300 °C for 5 h. The calcined BCTZ powders were subsequently ball-milled for 96 h and sieved at 200 μm.

Dense samples (labelled as D) were produced by uniaxial pressing into disk with a pressure of 100 MPa followed by cold-isostatic pressing at 300 MPa. The sintering was carried out in a covered ZrO_2 box at 1500 °C for 4 h, with natural cooling in the furnace. For porous samples (labelled as P), 55 vol. % rice starch (Aldrich, theoretical density of 1.43 g/cm^3) was used as a pore-forming agent. The starch was mixed with the BCTZ powders in a roller bottle for 30 min, sieved at 40 μm, and then shaped and sintered under the same conditions as the dense samples. The density of the sintered samples was measured using the Archimedes method and reported in Table 1 together with the labels and the dimensions. The relative density was calculated based on theoretical density of 5.68 g/cm^3 [98].

X-ray powder diffraction (XRPD) analysis, performed using a Bruker D8 Advance X-ray diffractometer (θ–θ) with Cu Kα radiation, confirmed the formation of pure perovskite structure (Fig. 1a) without any secondary phases (Fig. 1b).

Microstructures were analyzed with Field-Emission Scanning Electron Microscopy (FESEM, mod. ΣigmaCarl Zeiss NTS Gmbh Öberkochen, Germany). Dense BCTZ showed a dense microstructure with less than 3 vol% of porosity (see Fig. 2a). The grains, around 2 μm in size, exhibited both intergranular fractures in the finer grains and transgranular fractures in the coarser ones (see inset of Fig. 1a). The porous BCTZ sample exhibited approximately 30 % porosity, with good grain adhesion (see Fig. 2b). The resin in the pores is due to preparation for polishing process, and occurs only in samples used for SEM imaging. This high porosity allowed the Ag to penetrate down to 100 μm of depth during sputtering (inset of Fig. 2b). Silver electrodes, approximately 250 nm thick, were sputtered onto the plane-parallel surfaces of the ceramic disks before the poling process.

Conventional oil-based poling was performed in a silicon oil bath under a DC field of 3 kV/mm for 30 min at RT. The piezoelectric response (d_{33}) was measured using a S 5865 Sinocera d_{33} meter, applying a sinusoidal mechanical load with an amplitude of 0.25 N at 110 Hz. The resulting d_{33} values were approximately 325 pC/N for dense specimens and 165 pC/N for porous specimens (see Fig. 3). It is worth noting that for thicker samples more than 23 kV was required, and discharge phenomena were observed.

The SEM-induced poling process was performed on samples with electrodes on both surfaces, ensuring no short circuits after sputtering. The edges of the samples were polished to remove any residual silver, and the samples were mounted on stubs using double-sided carbon tape. Poling was performed under a vacuum of 0.2 Pa using an accelerating voltage of 20 kV, a 120 μm aperture and TV scanning mode. A probe current of about 9 nA was measured through a Faraday cage, while the specimen current passed across the specimens was around 5 nA. No significant differences in the d_{33} coefficient were observed when varying the scan speed (from 21.6 min to 122.3 ms per scan), magnification or working distance (from 1 mm to 45 mm). However, a gradual increase of

Table 1
Geometrical characteristic values for dense (D) and porous (P) samples with thin (t subscript) or thick (T subscript) thickness.

Sample (ID)	Diameter (mm)	Thickness (mm)	Density (g/cm^3)	Relative density (%)
D_t	10.6	1.4	5.57	98
D_T	7.9	8.4	5.65	99
D_t*	10.5	1.4	5.64	99
D_t°	10.5	1.4	5.62	99
P_T	7.7	9.3	4.20	74

* Sample without the electrode on the surface that was entirely scanned by the electron-beam.

° Sample without the electrode, poled by focusing the electron beam on a spot at the center of the sample.

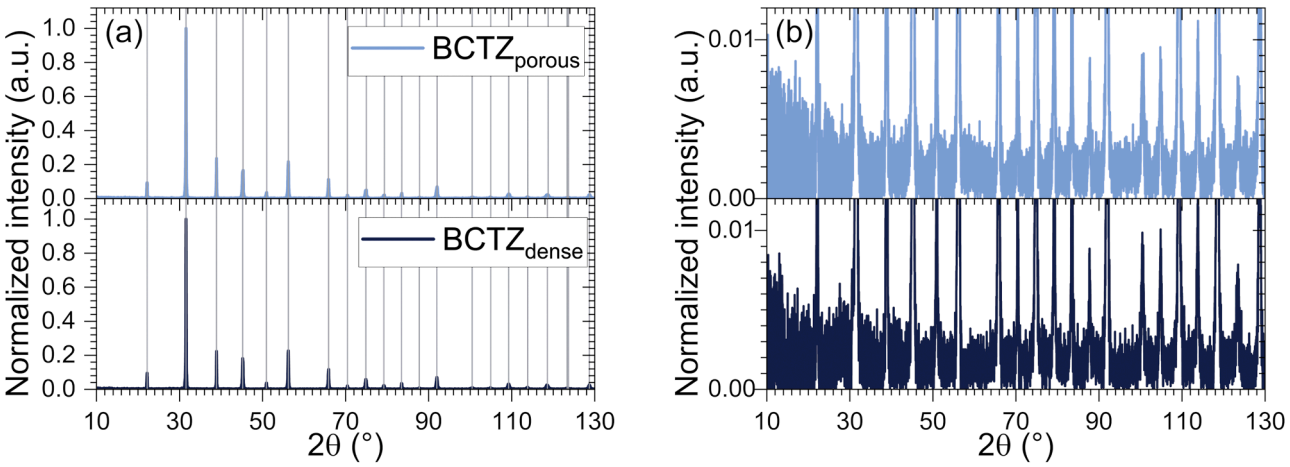

Fig. 1. (a) Normalized X-ray powder diffraction (XRPD) patterns of pulverized $BCTZ_{dense}$ (bottom) and $BCTZ_{porous}$ (top) samples, with peaks' positions marked by gray vertical lines. (b) Magnified view (from 0 to 0.012) of the normalized XRPD intensities for the dense (bottom) and porous (top) BCTZ samples.

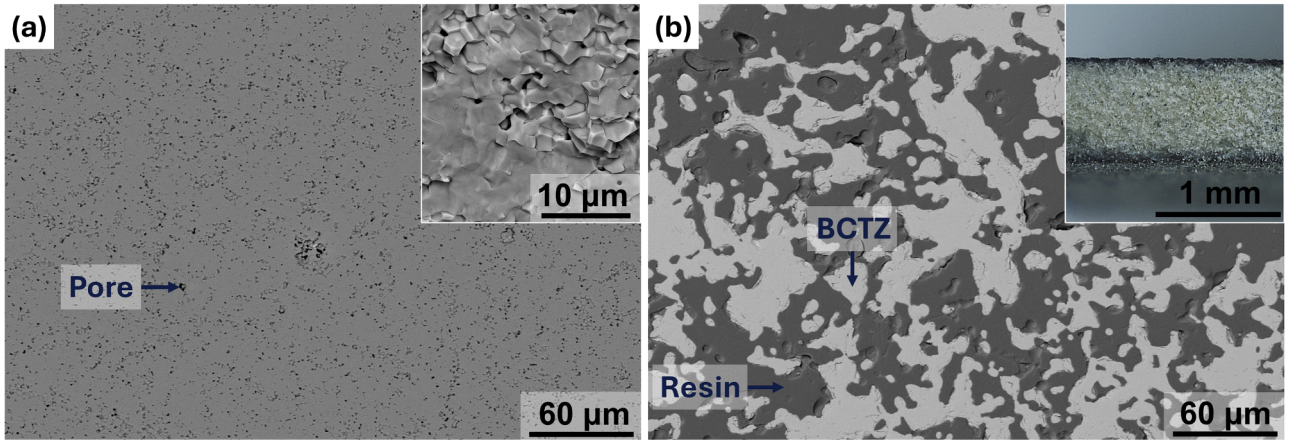

Fig. 2. SEM micrographs of polished surfaces of (a) dense and (b) porous BCTZ samples. The inset in (a) is a SEM micrograph of fracture surface of dense BCTZ. The inset in (b) is an optical micrograph of a piece of porous BCTZ cross section after Ag sputtering.

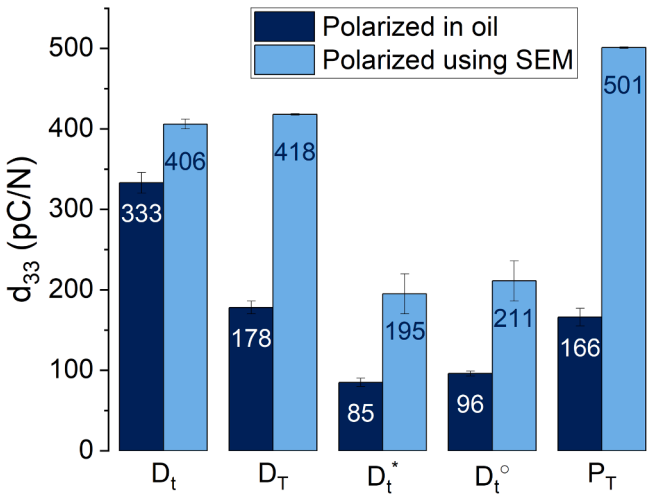

Fig. 3. d_{33} after poling in oil (blu bars) or SEM-induced polarization (azure bars) for dense (D) and porous (P) samples with thin (t) or thick (T) thickness. The D_t* sample lacked the electrode on the surface that was entirely scanned by the electron-beam, while the D_t° sample was poled by focusing the electron beam on a spot at its center without an electrode. For the latter sample, the d_{33} was measured at the polarized spot.

d_{33} was observed as the exposure time increased from 20 to 60 min, leading to full poling for both dense and porous samples. These results are consistent with previous studies on charge accumulation induced by SEM. It is well established that when an electron beam of sufficient energy irradiates the surface of a good insulator, the charge density and surface potential increase linearly with time until the breakdown potential is reached [99]. Exceptionally higher d_{33} values obtained with SEM-induced poling compared to conventional oil-based poling (Fig. 3) demonstrate the potential for full poling using SEM, highlighting its advantages over traditional oil-based methods, where discharge phenomena frequently occur, particularly at high voltages. In fact, as reported in the literature, when the electric field exceeds a certain threshold, polarization saturates and further increases in the field can lead to local overheating, microstructural damage, and even thermal breakdown, ultimately degrading the piezoelectric response [100,101]. SEM-induced poling appears to be a self-limiting technique. Once the maximum charge density and surface potential reaches the breakdown potential, the leakage current does not damage the material, unlike the oil-based method. No signs of damage were observed after SEM-induced poling, whereas in oil-based poling, discharges led to visible damage, including electrode erosion and dark pathways along the sample's side surfaces. The d_{33} response was halved when the BCTZ samples were polarized by directly applying the electron beam to the bare surface. This reduction occurred both when the entire surface was scanned (sample D_t*) and when the beam was focused on a localized area

(sample D_t°). The reduced d_{33} may be attributed to the bare surface's lower ability to trap electrons and holes [102]. In the case of sample D_t°, the d_{33} dropped to 0 pC/N when measurements were taken far from the irradiated area, demonstrating the possibility to selectively polarize specific regions of the sample. This level of spatial control is not achievable with corona poling, further highlighting one of the key advantages of SEM-induced poling. From the perspective of the d_{33}-meter, all samples showed a negatively poled irradiated surface, meaning the electric dipole moment pointed upward: from the bottom surface (negatively charged, depleted of electrons during poling) toward the irradiated surface (positively charged, the electron-rich side). For further details, see the "Piezoelectric effect direction: an apparent inversion" section in the support information. Finally, the piezoelectric response from SEM-induced poling was found to degrade at a similar rate to that of oil-poled specimens over a period of 200 days, demonstrating that the stability of the polarization induced by SEM is comparable to that of conventional poling.

This study investigates electron-beam poling method that extends the versatility of the poling process for ferroelectric materials enabling previously unachievable precision in polarizing intricate materials and structures. A key advantage of the SEM poling technique is that it allows the polarization of ferroelectric materials without requiring electrodes and it allows to polarize porous structures without inducing discharge phenomena. This opens possibilities for polarizing ferroelectric powders, ferroelectric photo-active semiconductors [103,104], specific patterns within ferroelectric components, thanks to the sub-micron spatial control achievable with the SEM. For example, it can be used to selectively polarize layered ferroelectric/ferromagnetic composites along surfaces where both ferroelectric and ferromagnetic stripes are visible. Another notable benefit is the widespread availability of SEM instruments in research laboratories and industrial R&D labs, along with the fact that this method avoids the use of oil, which hinder some biomedical applications or compromise components, such as reducing the wettability of membranes [89]. In future work, SEM-induced poling will be studied in greater detail to better understand the underlying physical principles and to explore how process parameters influence the polarization of various ferroelectric materials, including other lead-free materials, as well as ferroelectric/ferromagnetic composites.

Funding

This work has been funded by the European Union – NextGenerationEU– Project SELWA – CUP B53D23008660006 - Grant Assignment Decree No 20229PNWM7.

CRediT authorship contribution statement

Pietro Galizia: Writing – review & editing, Writing – original draft, Visualization, Validation, Supervision, Resources, Project administration, Methodology, Investigation, Funding acquisition, Data curation, Conceptualization. **Alessia Tavolaro:** Validation, Investigation. **Carlo Baldisserri:** Writing – review & editing, Validation, Resources, Methodology. **Floriana Craciun:** Writing – review & editing, Supervision, Methodology. **Elisa Mercadelli:** Writing – review & editing, Resources, Project administration.

Declaration of competing interest

The authors declare that they have no known competing financial interests or personal relationships that could have appeared to influence the work reported in this paper.

Supplementary materials

Supplementary material associated with this article can be found, in the online version, at doi:10.1016/j.scriptamat.2025.116795.

References

[1] J. Zhang, S. Ye, H. Liu, X. Chen, X. Chen, B. Li, W. Tang, Q. Meng, P. Ding, H. Tian, X. Li, Y. Zhang, P. Xu, J. Shao, Nano Energy 77 (2020) 105300.
[2] D. Li, R. Qin, J. Xu, J. Zhou, B. Chen, Acta Mech. Solida Sin. 35 (2022) 1004–1020.
[3] Y. Huang, W. Guo, J. Jia, L. Wang, S. Yin, Acta Mech. Solida Sin. 34 (2021) 862–871.
[4] C. Yang, F. Chen, J. Sun, N. Chen, ACS Omega 6 (2021) 30769–30778.
[5] F. Craciun, F. Cordero, E. Mercadelli, N. Ilic, C. Galassi, C. Baldisserri, J. Bobic, P. Stagnaro, G. Canu, M.T. Buscaglia, A. Dzunuzovic, M.V. Petrovic, Compos. B: Eng. 263 (2023) 110835.
[6] M.V. Petrovic, F. Craciun, F. Cordero, E. Mercadelli, N. Ilic, Z. Despotovic, J. Bobic, A. Dzunuzovic, C. Galassi, P. Stagnaro, G. Canu, M.T. Buscaglia, E. Brunengo, Polym. Compos. 45 (2024) 4428–4446.
[7] H. Cui, R. Hensleigh, D. Yao, D. Maurya, P. Kumar, M.G. Kang, S. Priya, X. (R) Zheng, Nat. Mater. 18 (2019) 234–241.
[8] C. Padurariu, L. Padurariu, L. Curecheriu, C. Ciomaga, N. Horchidan, C. Galassi, L. Mitoseriu, Ceram. Int. 43 (2017).
[9] K. Didilis, D. Marani, U.D. Bihlet, A.B. Haugen, V. Esposito, Addit. Manuf. 60 (2022) 103197.
[10] M. Mariani, R. Beltrami, E. Migliori, L. Cangini, E. Mercadelli, C. Baldisserri, C. Galassi, N. Lecis, J. Eur. Ceram. Soc. 42 (2022) 5598–5605.
[11] Q. Jiang, J. Guo, M. Nie, X. Zhu, H. Zhang, ACS Appl. Electron. Mater. 5 (2023) 6355–6361.
[12] F. Bertolini, M. Mariani, E. Mercadelli, C. Baldisserri, C. Galassi, C. Capiani, R. Ardito, N. Lecis, J. Mater. Res. Technol. 29 (2024) 4597–4606.
[13] Y. Liu, L. Zhao, L. Wang, H. Zheng, D. Li, R. Avila, K.W.C. Lai, Z. Wang, Z. Xie, Y. Zi, X. Yu, Adv. Mater. Technol. 4 (2019) 1900744.
[14] H. Yang, X. Yao, Z. Zheng, L. Gong, L. Yuan, Y. Yuan, Y. Liu, Compos. Sci. Technol. 167 (2018) 371–378.
[15] D. Zou, H. Mao, Z. Zhong, Ceram. Int. 48 (2022) 7362–7373.
[16] T. Samma, T. Fuchigami, S. Nakamura, T. Fey, K. Kakimoto, Phys. Status Solidi (b) 259 (2022) 2100611.
[17] H. Sugimoto, J. Biggemann, T. Fey, P. Singh, D. Khare, A.K. Dubey, K. Kakimoto, Mater. Lett. 297 (2021) 129969.
[18] F. Yang, Y. Zhao, Nano Energy 131 (2024) 110270.
[19] K. Coleman, J. Walker, W. Zhu, S.W. Ko, P. Mardilovich, S. Trolier-McKinstry, in: 2020 Joint Conference of the IEEE International Frequency Control Symposium and International Symposium on Applications of Ferroelectrics (IFCS-ISAF), 2020, pp. 1–5.
[20] M. Sadeqi-Moqadam, J. Glaum, Colloids Surf. A: Physicochem. Eng. Asp. 688 (2024) 133569.
[21] K.K. Poon, M.C. Wurm, D.M. Evans, M.-A. Einarsrud, R. Lutz, J. Glaum, J. Biomed. Mater. Res. B: Appl. Biomater. 108 (2020) 1295–1303.
[22] M. Moreau, A. Marthinsen, S.M. Selbach, T. Tybell, Phys. Rev. B 96 (2017) 094109.
[23] H. Abdolmaleki, A.B. Haugen, Y. Merhi, J.V. Nygaard, S. Agarwala, Mater. Today Electron. 5 (2023) 100056.
[24] I. Efe, N.A. Spaldin, C. Gattinoni, J. Chem. Phys. 154 (2021) 024702.
[25] A.R. Jayakrishnan, V.B. Isfahani, S.K.P. Nair, K.C. Sekhar, L.S. Marques, M. Pereira, J.L. MacManus-Driscoll, J.P.B. Silva, J. Energy Storage 97 (2024) 112846.
[26] I. Babu, G. de With, Compos. Sci. Technol. 91 (2014) 91–97.
[27] P. Galizia, C.E. Ciomaga, L. Mitoseriu, C. Galassi, J. Eur. Ceram. Soc. 37 (2017) 161–168.
[28] P. Galizia, M. Algueró, N. Bernier, N. Gambacorti, E. Aza, A. Lappas, M. Venet, C. Galassi, J. Alloys Compd. 783 (2019) 237–245.
[29] S. Karmakar, R. Kiran, C. Bowen, R. Vaish, V.S. Chauhan, Z.M. Elqahtani, S. B. Ahmed, M.S. Al-Buriahi, A. Kumar, T.H. Sung, Sci. Rep. 12 (2022) 22610.
[30] A. Iacomini, M. Koblar, H. Uršič, T. Rojac, J. Eur. Ceram. Soc. 44 (2024) 6948–6959.
[31] I. Coondoo, J. Vidal, I. Bdikin, R. Surmenev, A.L. Kholkin, Ceram. Int. 48 (2022) 24439–24453.
[32] J.M. Marshall, Q. Zhang, R.W. Whatmore, Thin Solid Films 516 (2008) 4679–4684.
[33] S.W. Konsago, K. Žiberna, A. Matavž, B. Mandal, S. Glinšek, Y. Fleming, A. Benčan, G.L. Brennecka, H. Uršič, B. Malič, ACS Appl. Electron. Mater. 6 (2024) 4467–4477.
[34] M. Billah, Y. Terasawa, M.K. Masud, T. Asahi, M.B.Z. Hegazy, T. Nagata, T. Chikyow, F. Uesugi, M.S.A. Hossain, Y. Yamauchi, Chem. Sci. 15 (2024) 9147–9154.
[35] P. Tipsawat, X. Zheng, Q.T. Tran, T.N. Jackson, S. Trolier-McKinstry, J. Appl. Phys. 136 (2024) 095101.
[36] H. Wang, J. Liu, S. Sadeghzade, R. Hou, H. Yuan, Ceram. Int. 49 (2023) 11334–11343.
[37] E.W. Yap, J. Glaum, J. Oddershede, J.E. Daniels, Scr. Mater. 145 (2018) 122–125.
[38] S. Smaranika Dani, A. Tripathy, N. Rao Alluri, S. Balasubramaniam, A. Ramadoss, Mater. Adv. 3 (2022) 8886–8921.
[39] M. Rotan, M. Zhuk, J. Glaum, J. Eur. Ceram. Soc. 40 (2020) 5402–5409.
[40] N. Yamamoto, Y. Yamashita, Y. Hosono, K. Itsumi, K. Higuchi, US20140062261 Ultrasonic probe, piezoelectric transducer, method of manufacturing Ultrasonic probe, and method of manufacturing piezoelectric transducer, US20140062261A1, n.d.
[41] W.-Y. Chang, C.-C. Chung, C. Luo, T. Kim, Y. Yamashita, J.L. Jones, X. Jiang, Mater. Res. Lett. 6 (2018) 537–544.

[42] Z. Zhang, J. Xu, L. Yang, S. Liu, J. Xiao, R. Zhu, X. Li, X. Wang, H. Luo, J. Appl. Phys. 125 (2019) 034104.
[43] K. Zhao, M. Zheng, X. Yan, M. Zhu, Y. Hou, J. Mater. Sci.: Mater. Electron. 32 (2021) 27815–27822.
[44] W. Liu, D. Ran, Y. Zhao, Y. Liang, R. Zhuo, S. Li, J. Alloys Compd. 1024 (2025) 180144.
[45] R. Roth, M.M. Koch, A.D. Rata, K. Dörr, Adv. Electron. Mater. 8 (2022) 2101416.
[46] K. Alhada–Lahbabi, D. Deleruyelle, B. Gautier, NPJ Comput. Mater. 10 (2024) 1–13.
[47] D. Schilling, S. Schuler, K. Dransfeld, in: 6th International Symposium on Electrets,(ISE 6) Proceedings, 1988, pp. 80–86.
[48] D. Schilling, K. Dransfeld, E. Bihler, K. Holdik, W. Eisenmenger, J. Appl. Phys. 65 (1989) 269–275.
[49] M. Fujimura, T. Suhara, H. Nishihara, Electron. Lett. 28 (1992) 721.
[50] M. Fujimura, K. Kintaka, T. Suhara, H. Nishihara, Electron. Lett. 28 (1992) 1868.
[51] H.A. Lu, L.A. Wills, B.W. Wessels, W.P. Lin, G.K. Wong, Appl. Phys. Lett. 63 (1993) 874–876.
[52] M. Houe, P.D. Townsend, J. Phys. D: Appl. Phys. 28 (1995) 1747.
[53] R. Danz, M. Pinnow, A. Buchtemann, A. Wedel, IEEE Trans. Dielectr. Electr. Insul. 5 (1998) 16–20.
[54] C. Restoin, C. Darraud-Taupiac, J.-L. Decossas, J.-C. Vareille, V. Couderc, A. Barthélémy, A. Martinez, J. Hauden Appl. Opt. AO 40 (2001) 6056–6061.
[55] J.H. Ferris, D.B. Li, S.V. Kalinin, D.A. Bonnell, Appl. Phys. Lett. 84 (2004) 774–776.
[56] Y. Glickman, E. Winebrand, A. Arie, G. Rosenman, Appl. Phys. Lett. 88 (2006) 011103.
[57] D. Li, D.A. Bonnell, Annu. Rev. Mater. Res. 38 (2008) 351–368.
[58] L.S. Kokhanchik, R.V. Gainutdinov, S.D. Lavrov, T.R. Volk, J. Appl. Phys. 118 (2015) 072001.
[59] A.A. Tatarintsev, K.E. Markovets, E.I. Rau, J. Phys. D: Appl. Phys. 52 (2019) 115104.
[60] L.S. Kokhanchik, E.V. Emelin, V.V. Sirotkin, Opt. Mater. 128 (2022) 112405.
[61] R. Schiek, T. Pertsch, Opt. Mater. Express OME 2 (2012) 126–139.
[62] T. Ichinokawa, M. Iiyama, A. Onoguchi, T. Kobayashi, Jpn. J. Appl. Phys. 13 (1974) 1272.
[63] C. Le Gressus, F. Valin, M. Gautier, J.P. Duraud, J. Cazaux, H. Okuzumi, Scanning 12 (1990) 203–210.
[64] S. Su, R. Zuo, S. Lu, Z. Xu, X. Wang, L. Li, Curr. Appl. Phys. 11 (2011) S120–S123.
[65] A. Reyes-Montero, L. Pardo, R. López-Juárez, A.M. González, M.P. Cruz, M. E. Villafuerte-Castrejón, J. Alloys Compd. 584 (2014) 28–33.
[66] F. Cordero, F. Craciun, P.S. da Silva, M.V. Zambrano, E. Mercadelli, P. Galizia, Phys. Rev. B 111 (2025) 054112.
[67] A. Reyes-Montero, F. Rubio-Marcos, L. Pardo, A.D. Campo, R. López-Juárez, M. E. Villafuerte-Castrejón, J. Mater. Chem. A 6 (2018) 5419–5429.
[68] V. Rojas, J. Koruza, E.A. Patterson, M. Acosta, X. Jiang, N. Liu, C. Dietz, J. Rödel, J. Am. Ceram. Soc. 100 (2017) 4699–4709.
[69] S. Patel, A. Chauhan, V. Rojas, N. Novak, F. Weyland, J. Rödel, R. Vaish, Energy Technol. 6 (2018) 872–882.
[70] G. Tutuncu, B. Li, K. Bowman, J.L. Jones, J. Appl. Phys. 115 (2014) 144104.
[71] M. Zakhozheva, L.A. Schmitt, M. Acosta, W. Jo, J. Rödel, H.-J. Kleebe, Appl. Phys. Lett. 105 (2014) 112904.
[72] H. Guo, C. Zhou, X. Ren, X. Tan, Phys. Rev. B 89 (2014) 100104.
[73] M. Nord, P.E. Vullum, I. Hallsteinsen, T. Tybell, R. Holmestad, Ultramicroscopy 169 (2016) 98–106.
[74] W. Liu, X. Ren, Phys. Rev. Lett. 103 (2009) 257602.
[75] D.R.J. Brandt, M. Acosta, J. Koruza, K.G. Webber, J. Appl. Phys. 115 (2014) 204107.
[76] R. Frey, B.F. Grosso, P. Fandré, B. Mächler, N.A. Spaldin, A.M Tehrani, Phys. Rev. Res. 5 (2023) 023122.
[77] M. Acosta, N. Novak, G.A. Rossetti Jr., J. Rödel Appl. Phys. Lett. 107 (2015) 142906.
[78] Y. Zhang, J. Glaum, M.C. Ehmke, J.E. Blendell, K.J. Bowman, M.J. Hoffman, J. Am. Ceram. Soc. 99 (2016) 174–182.
[79] N.S.K. Kumar, A.R. Jayakrishnan, J.P.B. Silva, K.C. Sekhar, Mater. Today Commun. 35 (2023) 105754.
[80] K. Nadaud, G.F. Nataf, N. Jaber, M. Bah, B. Negulescu, P. Andreazza, P. Birnal, J. Wolfman, Appl. Phys. Lett. 124 (2024) 042901.
[81] J.G. Maier, A. Gadelmawla, N.H. Khansur, K.G. Webber, J. Mater. 9 (2023) 673–682.
[82] N.D. Scarisoreanu, F. Craciun, A. Moldovan, V. Ion, R. Birjega, C. Ghica, R. F. Negrea, M. Dinescu, ACS Appl. Mater. Interfaces 7 (2015) 23984–23992.
[83] Y. Saito, H. Takao, T. Tani, T. Nonoyama, K. Takatori, T. Homma, T. Nagaya, M. Nakamura, Nature 432 (2004) 84–87.
[84] D. Liu, L.-F. Zhu, T. Tang, J.-R. Li, L. Wang, Y.-X. Liu, J. Hao, S. Wang, K. Wang, ACS Appl. Mater. Interfaces 16 (2024) 7444–7452.
[85] G. Huangfu, J. Wang, H. Zhang, J. Chen, Z. Liu, Y. Guo, Nano Lett. 24 (2024) 12148–12155.
[86] Y. Bai, A. Matousek, P. Tofel, V. Bijalwan, B. Nan, H. Hughes, T.W. Button, J. Eur. Ceram. Soc. 35 (2015) 3445–3456.
[87] K. Castkova, K. Maca, J. Cihlar, H. Hughes, A. Matousek, P. Tofel, Y. Bai, T. W. Button, J. Am. Ceram. Soc. 98 (2015) 2373–2380.
[88] Z. Hanani, S. Merselmiz, M. Amjoud, D. Mezzane, M. Lahcini, J. Ghanbaja, M. Spreitzer, D. Vengust, M. El Marssi, I.A. Luk'yanchuk, Z. Kutnjak, B. Rožič, M. Gouné, J. Mater. 8 (2022) 873–881.
[89] D.K. Dobesh, A. Gadelmawla, H. Miyazaki, M. Hinterstein, K. Kimura, J.G. Maier, S. Banerjee, O. Zeair, S.C. Mehta, L.L. da Silva, N.H. Khansur, K. Hayashi, D. de Ligny, K.G. Webber, M.R. Cicconi, J. Eur. Ceram. Soc. 44 (2024) 5646–5658.
[90] M. Kuhfuß, J.G. Maier, D.A. Hall, B. Xie, A.K. Kleppe, A. Martin, K. Kakimoto, N. H. Khansur, K.G. Webber, J. Appl. Phys. 135 (2024) 174101.
[91] J.G. Maier, M. Kuhfuß, D. Urushihara, A. Gadelmawla, N.H. Khansur, D. Hall, M. Algueró, A. Martin, K. Kakimoto, K.G. Webber, Ceram. Int. 50 (2024) 26780–26791.
[92] A. Martin, N. Kato, T. Fey, K.G. Webber, K. Kakimoto, Jpn. J. Appl. Phys. 63 (2024) 09SP02.
[93] F. Cordero, F. Craciun, M. Dinescu, N. Scarisoreanu, C. Galassi, W. Schranz, V. Soprunyuk, Appl. Phys. Lett. 105 (2014) 232904.
[94] V. Ion, F. Craciun, N.D. Scarisoreanu, A. Moldovan, A. Andrei, R. Birjega, C. Ghica, F. Di Pietrantonio, D. Cannata, M. Benetti, M. Dinescu, Sci. Rep. 8 (2018) 2056.
[95] C. Bantignies, R. Rouffaud, G. Buse, P. Veber, H. Cabane, A. Borta-Boyon, M. P. Thi, P. Mauchamp, A. Lejeune, M. Maglione, L. Colin, A. Balé, M. Flesch, F. Levassort, IEEE Trans. Ultrason. Ferroelectr. Freq. Control 71 (2024) 27–37.
[96] J. Gao, Z. Zhu, M. Qiu, X. Chen, Y. Fan, J. Environ. Chem. Eng. 12 (2024) 112105.
[97] K.G. Webber, O. Clemens, V. Buscaglia, B. Malič, R.K. Bordia, T. Fey, U. Eckstein, J. Eur. Ceram. Soc. 44 (2024) 116780.
[98] K. Orlik, Y. Lorgouilloux, P. Marchet, A. Thuault, F. Jean, M. Rguiti, C. Courtois, J. Eur. Ceram. Soc. 40 (2020) 1212–1216.
[99] X. Tang, D.C. Joy, Scanning 26 (2004) 226–234.
[100] T. Lu, H. Du, N. Kong, H. Li, S. Xu, Z. Li, X. Du, J. Mater. Sci.: Mater. Electron. 34 (2023) 797.
[101] Y. Liu, X. Du, H. Zhang, Y. Li, H. Du, Ceram. Int. 51 (2025) 6430–6438.
[102] Z.J. Ding, C. Li, B. Da, J. Liu, Sci. Technol. Adv. Mater. 22 (2021) 932–971.
[103] S. Casadio, A. Gondolini, N. Sangiorgi, A. Candini, A. Sanson, Sustain. Energy Fuels 7 (2023) 1107–1118.
[104] L. Liu, H. Huang, Z. Chen, H. Yu, K. Wang, J. Huang, H. Yu, Y. Zhang, Angew. Chem. Int. Ed. 60 (2021) 18303–18308.